ADVANCED QUANTUM TECHNOLOGIES
www.advquantumtech.com

Mid-Infrared Sensing Using a Hollow–Core Fiber in a Nonlinear Interferometer

*Thomas Produit, Tanmoy Chakraborty, Ang Deng, Leonid Krivitsky, Wonkeun Chang, and Anna V. Paterova**

Increasing the interaction path length is a well-known method for enhancing the sensitivity of the optical detection system. Hollow–core fibers (HCFs) represent a viable alternative to the traditional multi-path cells offering low optical losses and strong confinement of the optical field. Here, the incorporation of an Antiresonant Hollow–core Fiber (AR-HCF) section into a nonlinear interferometer, where the AR-HCF section serves as a gas-sensing cell operating in the IR range is presented. By exploiting the effect of nonlinear interference, the detection is brought into the more operation-friendly visible range. The detection of methane (CH_4) gas at mid-IR wavelengths within a half-meter section of AR-HCF, with an estimated concentration accuracy of 200 ppm·m is demonstrated. These results represent the combination of two research fields within a single instrument and pave the way for further advancement of quantum-inspired gas sensing techniques.

1. Introduction

The ability to measure minute concentrations of gases is crucial for multiple areas of strategic importance, including medical diagnostics,[1] environmental monitoring,[2] and industrial applications.[3] Conventional methods of gas sensing use a mid-infrared (mid-IR) light source, tuned to resonance absorption lines of the gas under study. The light interacts with the gas in a multi-path cell (MPC), and the concentration of the gas is inferred from the light attenuation measured by a mid-IR photodetector, following Beer–Lamber law.[4] However, the reliability and sensitivity of these methods are hindered by the opto-mechanical and thermal drifts of MPCs.[5] An alternative approach is based on using hollow–core fibers (HCFs), whose core is filled with the gas while guiding the probing light through. Low optical losses and strong confinement of the optical field in the HCF enhance the interaction strength of the IR light with the gas. Among many types of HCFs, the most promising one for gas sensing is the anti-resonant HCFs (AR-HCFs).[6–8] This type of fiber has broadband guidance and a large diameter of the central hollow core, which leads to shorter gas exchange time. AR-HCFs have already been demonstrated for gas sensing experiments,[9–12] where several meters of interaction path length were achieved.[11] Specifically in the mid-IR, recent spectroscopic results have shown impressive sensitivity using AR-HCF as gas cells,[13] but these geometries still require specialized detectors tailored to detect mid-IR photons, like Mercury Cadmium Telluride (HgCdTe, MCT) detectors. These detectors are expensive, less sensitive than detectors in the visible, and often require cooling for proper functionality, as they suffer from thermal noise at ambient temperatures.[14]

An alternative to the scheme with direct detection of mid-IR light can be based on using the principles of nonlinear optical processes like sum-frequency generation[15,16] or using interference of correlated photons pairs.[17–19] However, the technique based on sum-frequency generation still requires powerful pump lasers, like Nd:YAG pulsed lasers, to drive the upconversion process and transform the probing IR beam to a detectable visible wavelength range. Moreover, these upconverting techniques also do not circumvent the need of an IR photon source at the first place, such as quantum cascade laser (QCL) or supercontinuum laser sources. The latter technique employing the interferometry of correlated photon pairs, known as "induced coherence without induced emission",[20–22] has already been demonstrated for applications in IR spectroscopy.[17–19] This technique allows obtaining information about sample's interaction with IR wavelengths by detecting correlated photons at conjugate visible or near-IR wavelengths through the

T. Produit, T. Chakraborty[+], L. Krivitsky, A. V. Paterova[++]
A*STAR Quantum Innovation Centre (Q.InC)
Institute of Materials Research and Engineering (IMRE)
Agency for Science
Technology and Research (A*STAR)
2 Fusionopolis Way, Innovis #08-03, Singapore 138634, Singapore
E-mail: paterovaav@susu.ac.ru

A. Deng, W. Chang
School of Electrical and Electronic Engineering
Nanyang Technological University
Singapore 639798, Singapore

A. Deng
College of Electronics and Information Engineering
Sichuan University
Chengdu, Sichuan 610064, China

The ORCID identification number(s) for the author(s) of this article can be found under https://doi.org/10.1002/qute.202400397

[+]Present address: Atomic, Molecular and Optical Physics Division, Physical Research Laboratory, Navrangpura, Ahmedabad 380009, India

[++]Present address: Laboratory of Quantum Engineering of Light, South Ural State University, Chelyabinsk 454080, Russia

DOI: 10.1002/qute.202400397

implementation of the nonlinear interferometry scheme. Thus, inferring sample properties at mid-IR (λ = 3–50 μm)[23] or even THz wavelengths[19,24] (λ = 100–1 mm)[25] can be performed using detectors for visible range. Furthermore, it is argued that these quantum techniques could achieve increased sensitivity in comparison with their classical counterparts.[26]

In this work, we combine our expertise in nonlinear interferometry with the use of HCFs for gas sensing measurements. We demonstrate the integration of an AR-HCF section into the nonlinear interferometry scheme. This allows increasing the optical path length of the probe beam through the gas under study. We report the sensing of methane gas (CH_4) at one of its absorption peaks via the detection of visible light, hence bypassing the need for mid-IR detectors. This approach demonstrates the combination of nonlinear interferometry and AR-HCF in a single instrument for gas detection measurements, expanding quantum-based sensing techniques.

2. Nonlinear Interferometry Using Stimulated Coherence

A nonlinear interferometry scheme implies using a source of correlated photons, commonly, generated via spontaneous parametric down-conversion (SPDC) in a nonlinear crystal. In this process, the laser pump photons annihilate, and correlated photon pairs, called signal and idler photons, are created. The wavelengths of the signal and idler photons can be tuned in the visible and mid-IR ranges, respectively, by changing the phase-matching conditions in the nonlinear crystal. Incorporating sequentially two of such nonlinear crystals with a common pump beam comprises a nonlinear interferometry scheme, where the superposition of SPDC state vectors results in an interference pattern. Thus, one can measure the losses at the IR range for idler photons propagating between crystals by detecting the intensity of the correlated signal photons I_s at the visible range. The resulting interference fringes depend on the intertwined relation of signal phase φ_s, idler phase φ_i and pump phase φ_p, given by:[20,21]

$$I_s \sim \left[1 + V \cdot \cos\left(\varphi_s + \varphi_i - \varphi_p\right)\right] \tag{1}$$

The visibility of the interference fringes V depends on the first-order correlation function $\mu(\Delta t)$ for SPDC photons and the amplitude transmission coefficient τ_i for idler photons at IR wavelengths range:

$$V = \mu\left(\Delta t\right)\ \left|\tau_i\right| = \mu\left(\Delta t\right) \exp\left(\frac{-\alpha_i L_i}{2}\right) \tag{2}$$

where α_i is the absorption coefficient at IR wavelengths, and L_i is the interaction length of the idler photons with the absorbing medium present in the interferometer. In this case, the first-order correlation function requires balancing the path lengths of the signal and idler photons in the interferometer within the coherence length of the SPDC photons.

To increase the visibility of the interference fringes in such a scheme it is possible to add seed photons with their wavelength and mode-matching idler photons. Indeed, the parametric down-conversion (PDC) in this case changes to the stimulated regime, where one of the SPDC modes is effectively enhanced.[27,28] In this regime, a non-linear relation arises between the interference visibility V' and the amplitude transmission coefficient τ_i of the sample,[29–33] which is given by:

$$V' = \frac{2\left|\tau_i\right|}{1 + \left|\tau_i\right|^2} \tag{3}$$

Moreover, the coherence length for stimulated PDC is then determined by the coherence length of the seed photons. Thus, using seed photons with a longer coherence length reduces the balancing constraints of the interferometer. This significantly simplifies the alignment of the system and allows integration of long fibers section in the IR arm, without the need to balance the pass length at the other arm of the interferometer. This can be particularly useful for long-distance gas sensing applications.[34]

3. Experimental Setup

3.1. Nonlinear Interferometer

We built a Michelson-type nonlinear interferometer, where only one nonlinear crystal is used, with the pump beam double passing through it, see **Figure 1**. The interferometer is built using a periodically poled lithium niobate (PPLN) nonlinear crystal (with poling periodicity of 10.73 μm), a continuous wave (CW) pump laser at 532 nm wavelength (Oxxius LCX-532) and a tunable Interband Cascade Laser CW seed laser at 3135–3559 nm (ICL BG-3.2-3.6, AlpesLaser SA), as sketched in Figure 1.

Using dichroic mirrors, the pump and seed lasers are directed into the nonlinear crystal, where non-degenerate stimulated PDC photon pairs can be generated at visible (signal photons, 635–624 nm) and corresponding IR wavelengths (idler photons, 3.29–3.608 μm). The phase matching conditions, and hence the idler/signal wavelengths, are tuned by controlling the temperature applied to the nonlinear crystal. Specifically, we set the temperature to $T = 56.0 \pm 0.1$ °C to ensure that the wavelength of the idler photons spectrally matches with one of the absorption lines of CH_4 gas at 3024 cm^{-1} (3.307 μm). Correspondingly, we set the seed laser to the same wavelength. Then, photons are split into two arms of the Michelson interferometer (visible and IR arms) according to their wavelengths by another dichroic mirror. Signal and pump photons propagate in free space, while idler and seed photons can either propagate in free space or be guided through the AR-HCF section of 53.5 ± 0.2 cm length (single pass). IR photons, once coupled in, are guided through the hollow core region of the fiber, which has a diameter of 85 μm. The suppression of mode coupling between the hollow core and the cladding ensures that light introduced into the core is effectively confined and transmitted along the fiber with minimal leakage. More detailed characteristics of the AR-HCF section are elaborated in Appendix A1.

Pump and signal photons (seed and idler) are then reflected back by the mirror M_s (M_i) into the nonlinear crystal through their initial path; hence the idler and seed photons pass again through the AR-HCF section. Mirror M_s is mounted onto the translation stage to introduce the additional phase into the interferometer. When the photons are recombined at the nonlinear

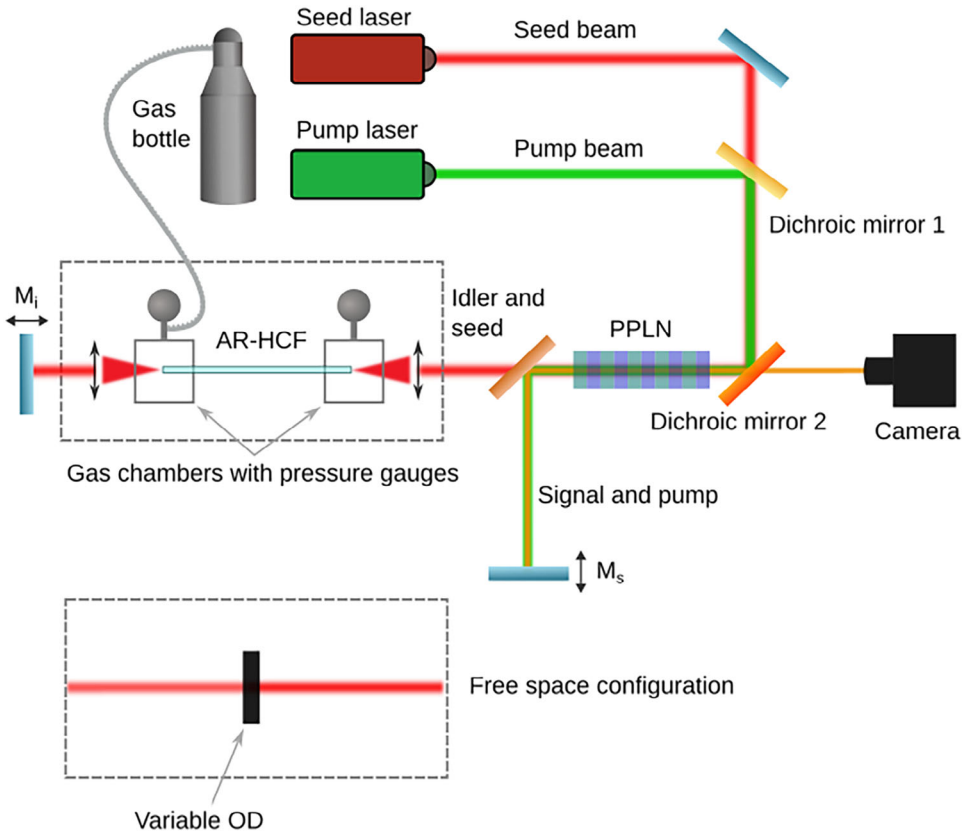

Figure 1. Schematic of the experimental setup. The IR arm of the interferometer can either incorporate the AR-HCF section or operate in a free space configuration, where a variable neutral density filter (OD) is introduced.

crystal, another stimulated PDC process takes place by the reflected pump and seed beams. Thus, interference of signal PDC photons generated at forward and backward passes through the nonlinear crystal is observed on the CMOS camera (Thorlabs Kiralux CS135MUN) operating at the visible range. Due to the relatively low losses of the AR-HCF and its polarization maintenance, the interference pattern of the signal photons is observed once the spatial modes for the signal and idler photons are aligned inside the interferometer.

To introduce gas into the system, we use custom-built gas housing cells at the ends of the AR-HCF and a gas delivery system. The gas delivery system (not shown here) works to feed different media and has separate gas lines: one for the vacuum pump, one for feeding the gas under study. One end of each gas cell has an IR window, which allows to couple IR light into the AR-HCF section, while the other end is glued to prevent any gas leakage. During the gas sensing measurements, first, we detect a reference interference pattern with AR-HCF section pumped down to vacuum pressures (down to ≈100 mPa). Then, we introduce the 2.5% methane and air gas mixture (CALGAZ ≤2.5%, Methane in Air: 18–22% O_2) into the AR-HCF, monitoring the pressure by a Bourgon gauge. Due to the absorption of the gas at IR range we observe altered interference fringes. As a result, by analyzing the change of the interference pattern, namely the visibility of the interference, we sense the concentration of the injected gas.

4. Results and Discussion

4.1. Interference Fringes with and Without Seeding

We study the stimulated regime of PDC generation by using the free space configuration of the IR arm of the interferometer. By introducing a variable step neutral density (ND) filter (Thorlabs NDL-25S-4 Step Variable ND Filter, OD: 0.1–4.0), we measure the interference visibility both for the seeded (≈150 μW power) and unseeded regimes of PDC generation. The resulting visibilities are presented as a function of transmittance at **Figure 2**a. For the unseeded case of PDC, the curve is given by a linear function, see Equation (2).[22] For the seeded PDC, the visibility of the interference fringes has a nonlinear relation depending on the transmittance in the IR arm of the interferometer, see Equation (3). Figure 2b shows interference fringes measured without introducing the ND filters. Although seeding induces an increase in visibility of the interference, due to a lack of active cavity stabilization of the seed laser, we experience slightly higher sensitivity to mechanical vibration in the seeded case. This results in the uncertainties of the interference visibility to be slightly higher, as shown in Figure 2. Moreover, the interference fringes exhibit a periodicity of 1.7 μm, as determined by the cosine fitting. This is half the wavelength of the seed laser, resulting from the double pass within the Michelson-type geometry of the interferometer. The maximum visibility of the interference fringes

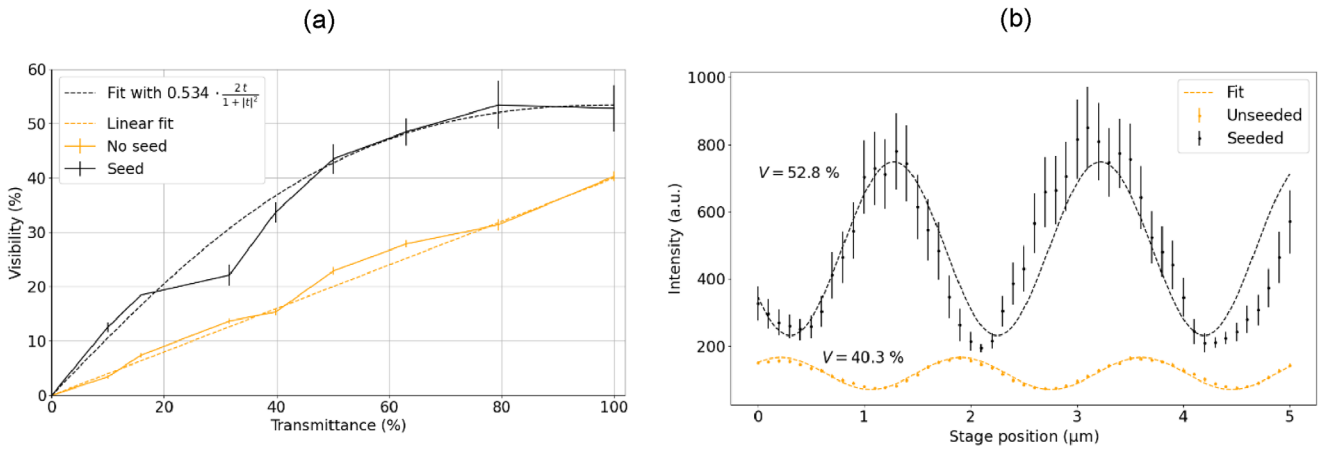

Figure 2. a) Comparison of the visibility of interference fringes at visible range with seeded (black) and unseeded (orange) PDC light source used in the nonlinear interferometer as a function of transmittance of IR photons. b) Example of interference fringes for signal photons at 634 nm (corresponding to 3.307 μm wavelength of the idler photons) depending on the position of mirror M_s. The upper fringes correspond to the interference observed at the CMOS camera for the seeded PDC case, and the fringes below correspond to the unseeded PDC case, correspondingly.

in spontaneous PDC is 40.3%, which is due to losses at the optical elements, and losses in all optical modes. In the stimulated PDC case, one of the modes is enhanced, which allows achieving 52.8% visibility of the interference fringes.

4.2. Mid-IR Gas Sensing Results

Next, we use the mid-IR seed laser to perform gas-sensing experiments. In these experiments, we introduce an AR-HCF gas cell in the IR arm of the nonlinear interferometer. The interference fringes are obtained using a seeding with the wavelength aligned with the absorption line of the CH_4 gas at 3024 cm^{-1} (3307 nm), corresponding to the detection of signal photons at 634 nm. In this case the interferometer arms do not require fine balancing like with unseeded PDC, since the coherence length is determined by the coherence of the seed laser, which corresponds to tens of meters.

We start the gas sensing measurements by pumping down the air pressure to vacuum inside the AR-HCF section to obtain the reference interference fringes, see **Figure** 3a. The visibility of the interference is reduced to 44.3% due to coupling losses into HCF, compared to initially 52.8% in the free space configuration of the IR arm of the interferometer. Next, we introduce the methane gas into the hollow core region of the fiber at different pressures of 70 and 90 kPa, which further reduces the visibility of the interference fringes due to the absorption of the gas. We take three measurements at each pressure value of the gas and calculate their average. Figure 3b,c shows the interference fringes obtained with AR-HCF gas cell filled with an air-CH_4 mixture (see full composition of the gas mixture in Appendix A3) at different pressures.

The results of the visibility measurements are presented in Figure 3d, where the visibility of the interference fringes drops with increasing pressure of the gas inside the hollow core region of the fiber. Since the visibility of the interferometric pattern is proportional to the absorption inside the AR-HCF gas cell, a reduction of visibility is used as means of sensing in the mid-IR. Given a visibility error of 1% and employing Equation (3) (see the full description in Appendix A2), we estimate the path-integrated sensitivity of this setup to be 2000 ppm·m. We obtained the fair sensitivity of the system, since we utilized the weaker absorption line at 3024 cm^{-1} in the experiment, see Figure S2 (Supporting Information) in Appendix A3. If the stronger absorption at 3067.2 cm^{-1} had been utilized, the estimated path-integrated sensitivity would be 200 ppm·m. This sensitivity is approximately two orders of magnitude lower than the detectivity reported in experiments using AR-HCF for Raman spectroscopy.[35] However, unlike that work, our system operates with two orders of magnitude less laser power and integrates 100 times faster. Additionally, compared to commercial systems, which typically achieve sensitivities on the order of tens of ppm, our system can achieve similar sensitivity by utilizing longer HCF sections. This value can be further improved even further by targeting other stronger absorption peaks, introducing a longer AR-HCF section, by reducing the interferometric noise or using a more powerful seed laser. Furthermore, the spectral resolution of our method is determined by the linewidth of the seed laser, which, based on our estimation, is better than 0.01 nm.

Additionally, our method allows gas specificity measurements via tuning the wavelength of the probe photons within the 3135–3559 nm range, facilitated by the tunability of the seed laser. One can also imagine pushing the spectral limits to 10 μm or beyond by employing other nonlinear crystals like for instance $AgGaS_2$ (AGS)[19,36] and corresponding seed sources. However, this technique does not require direct detection of mid-IR light, relying instead on available off-the-shelf components for visible light.

Our work, among others, proposes an extension to geometries and capabilities of the nonlinear interferometry schemes using hollow core fibers.[37] The use of HCFs brings significant flexibility to the setup, enabling the exploration and implementation of various interferometry schemes. For instance, IR optical coherence tomography[38–40] with HCFs may hold significant promise for imaging of bio-tissues, especially in applications for live-sensing/imaging.

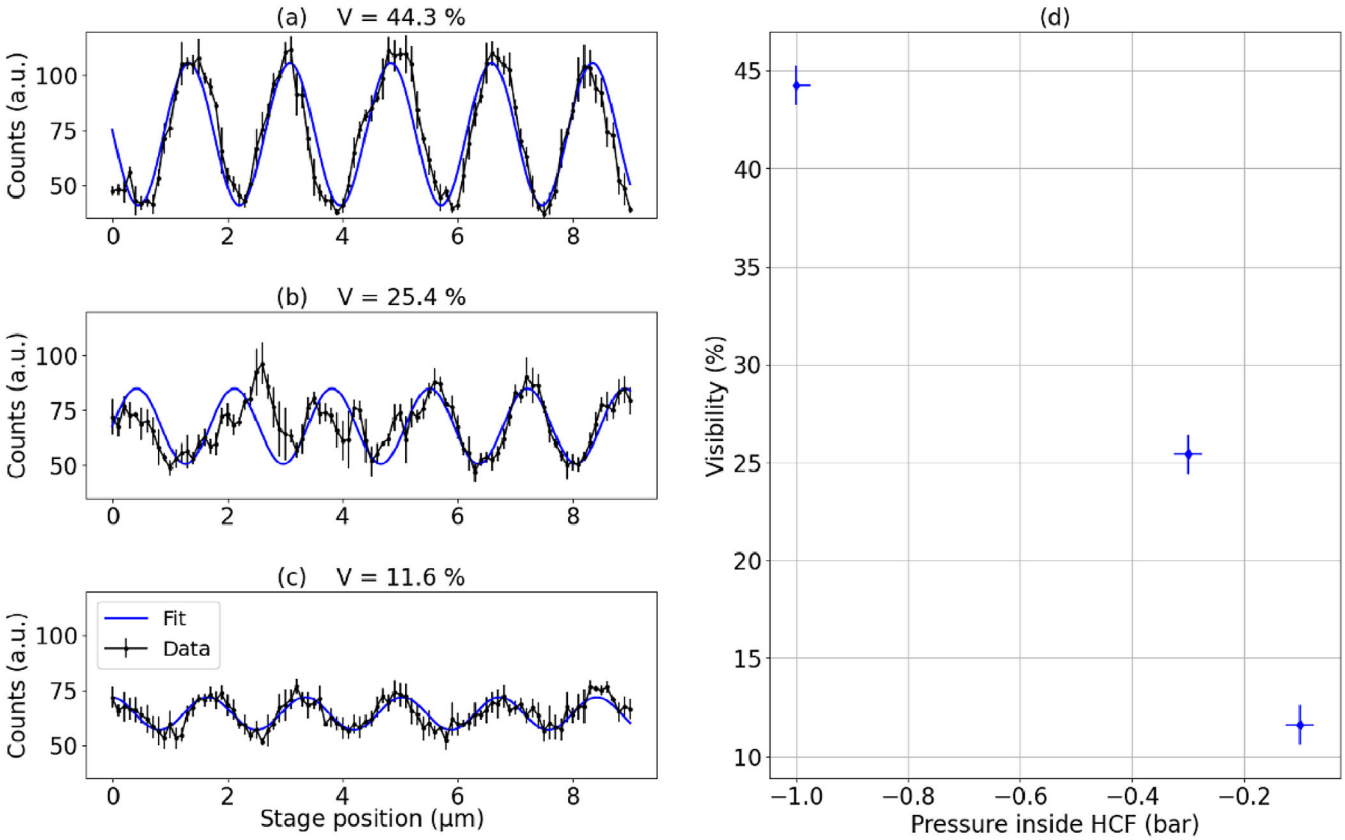

Figure 3. a) Reference interference fringes corresponding the AR-HCF filled with vacuum. Interference fringes corresponding to AR-HCF filled b) with an air-CH_4 gas mixture at an absolute pressure of P = 70 kPa, c) with an air-CH_4 gas mixture at an absolute pressure of P = 90 kPa. d) The visibility of the interference fringes depending on the pressure of the gas introduced into HCF.

5. Conclusion

In conclusion, we utilized a nonlinear interferometry method integrated with an AR-HCF section for gas sensing measurements. This innovative approach enables the detection of gases with mid-IR features using only a visible detector by observing the reduction in visibility, which correlates to gas absorption. We report the sensing of methane gas (CH_4) at one of its absorption peaks at 3024 cm^{-1} (3307 nm) via the detection of visible light at 634 nm wavelength, hence bypassing the need of mid-IR detectors. We estimate 200 ppm·m sensitivity of our method using an HCF section of 53 cm length, which can be increased further by using longer fiber sections. Our work demonstrates the successful combination of nonlinear interferometry and AR-HCF for gas detection, marking a significant advancement over earlier methods that relied on bulk optics and free-space IR light propagation. This limitation is effectively addressed by the inclusion of AR-HCF in our setup, paving the way for further innovations in nonlinear interferometry.

Supporting Information

Supporting Information is available from the Wiley Online Library or from the author.

Acknowledgements

T.P., T.Ch., and A.V.P acknowledge the support from the Agency for Science, Technology and Research (A*STAR) via grant funding no. C230917004, Q.InC Strategic Research and Translational Thrust and AME YIRG 2021 grant funding no. A2084c0178.

Conflict of Interest

The authors declare no conflict of interest.

Data Availability Statement

The data that support the findings of this study are available from the corresponding author upon reasonable request.

Keywords

mid-infrared sensing, nonlinear interferometry, quantum

Received: August 16, 2024
Revised: October 11, 2024
Published online: November 5, 2024

[1] B. Henderson, A. Khodabakhsh, M. Metsälä, I. Ventrillard, F. M. Schmidt, D. Romanini, G. A. Ritchie, S. L. Hekkert, R. Briot, T. Risby, N. Marczin, F. J. M. Harren, S. M. Cristescu, *Appl. Phys. B: Lasers Opt.* **2019**, *124*, 161.
[2] J. Jágerská, P. Jouy, B. Tuzson, H. Looser, M. Mangold, P. Soltic, A. Hugi, R. Brönnimann, J. Faist, L. Emmenegger, *Opt. Express* **2015**, *23*, 1512.
[3] H. Moser, W. Pölz, J. P. Waclawek, J. Ofner, B. Lendl, *Anal. Bioanal. Chem.* **2017**, *409*, 729.
[4] J. M. Hollas, *Modern Spectroscopy*, Wiley, Hoboken, NJ, USA **2003**.
[5] W. Ye, C. Zheng, N. P. Sanchez, A. V. Girija, Q. He, H. Zheng, R. J. Griffin, F. K. Tittel, *Infrared Phys. Technol.* **2018**, *89*, 299.
[6] F. Yu, J. C. Knight, *IEEE J. Sel. Top. Quantum Electron.* **2016**, *22*, 146.
[7] Md. I. Hasan, N. Akhmediev, W. Chang, *J. Lightwave Tech.* **2018**, *36*, 4060.
[8] A. Deng, W. Chang, *Crystals* **2021**, *11*, 420.
[9] M. Nikodem, G. Gomółka, M. Klimczak, D. Pysz, R. Buczyński, *Opt. Express* **2019**, *27*, 14998.
[10] M. Nikodem, G. Gomółka, M. Klimczak, D. Pysz, R. Buczyński, *Opt. Express* **2019**, *27*, 36350.
[11] K. Krzempek, K. Abramski, M. Nikodem, *Sensors* **2019**, *19*, 3352.
[12] P. Jaworski, *Sensors* **2021**, *21*, 5640.
[13] D. Tomaszewska-Rolla, P. Jaworski, D. Wu, F. Yu, A. Foltynowicz, K. Krzempek, G. Soboń, *Opt. Express* **2024**, *32*, 10679.
[14] G. Deng, W. Yang, X. Gong, Y. Zhang, *Infrared Phys. Technol.* **2020**, *105*, 103260.
[15] J. Fang, K. Huang, R. Qin, Y. Liang, E. Wu, M. Yan, H. Zeng, *Nat. Commun.* **2024**, *15*, 1811.
[16] Y. Cai, Y. Chen, K. Dorfman, X. Xin, X. Wang, K. Huang, E. Wu, *Sci. Adv.* **2024**, *10*, eadl3503.
[17] D. A. Kalashnikov, A. V. Paterova, S. P. Kulik, L. A. Krivitsky, *Nat. Photonics* **2016**, *10*, 98.
[18] C. Lindner, S. Wolf, J. Kiessling, F. Kühnemann, *Opt. Express* **2020**, *28*, 4426.
[19] A. V. Paterova, Z. S. D. Toa, H. Yan, L. A. Krivitsky, *ACS Photonics* **2022**, *9*, 2151.
[20] L. J. Wang, X. Y. Zou, L. Mandel, *Phys. Rev. A* **1991**, *44*, 4614.
[21] X. Y. Zou, L. J. Wang, L. Mandel, *Phys. Rev. Lett.* **1991**, *67*, 318.
[22] A. Hochrainer, M. Lahiri, M. Erhard, M. Krenn, A. Zeilinger, *Rev. Mod. Phys.* **2022**, *94*, 025007.
[23] "Optics and photonics – Spectral band", ISO 20473, **2007**, First Edition. https://www.iso.org/standard/39482.html
[24] M. Kutas, B. E. Haase, F. Riexinger, J. Hennig, P. Bickert, T. Pfeiffer, M. Bortz, D. Molter, G. von Freymann, *Adv. Quantum Technol.* **2022**, *5*, 2100164.
[25] Recommendation ITU-R V.431-8 (08/2015), "Nomenclature of the frequency and wavelength bands used in telecommunications", International Telecommunication Union. https://www.itu.int/dms_pubrec/itu-r/rec/v/R-REC-V.431-8-201508-I!!PDF-E.pdf.
[26] G. B. Lemos, M. Lahiri, S. Ramelow, R. Lapkiewicz, W. N. Plick, *J. Opt. Soc. Am. B* **2022**, *39*, 2200.
[27] Z. Y. Ou, L. J. Wang, X. Y. Zou, L. Mandel, *Phys. Rev. A.* **1990**, *41*, 1597.
[28] P. H. Souto Ribeiro, S. Padua, J. C. Machado da Silva, G. A. Barbosa, *Phys. Rev. A.* **1995**, *51*, 1631.
[29] A. Heuer, R. Menzel, P. W. Milonni, *Phys. Rev. A* **2015**, *92*, 033834.
[30] A. C. Cardoso, L. P. Berruezo, D. F. Ávila, G. B. Lemos, W. M. Pimenta, C. H. Monken, P. L. Saldanha, S. Pádua, *Phys. Rev. A* **2018**, *97*, 033827.
[31] S. K. Lee, T. H. Yoon, M. Cho, *Opt. Express* **2019**, *27*, 14853.
[32] Y. Michael, I. Jonas, L. Bello, M.-E. Meller, E. Cohen, M. Rosenbluh, A. Pe'er, *Phys. Rev. Lett.* **2021**, *127*, 173603.
[33] J. Florez, E. Pearce, N. R. Gemmell, Y. Ma, G. Bressanini, C. C. Phillips, R. F. Oulton, A. S. Clark, (Preprint) arXiv, arXiv:2209.06749v2.
[34] A. C. Cardoso, J. Dong, H. Zhou, S. K. Joshi, J. G. Rarity, (Preprint) arXiv, arXiv:2209.15289v2.
[35] M. Yang, Z. Liu, L. Xiong, Q. Nie, Y. Wang, S. Gao, M. Cheng, D. Yang, S. Pei, D. Guo, *Opt. Express* **2024**, *32*, 4093.
[36] Y. Mukai, R. Okamoto, S. Takeuchi, *Opt. Express* **2022**, *30*, 22624.
[37] S. Lopez-Huidobro, M. Noureddin, M. V. Chekhova, N. Y. Joly, *Opt. Lett.* **2023**, *48*, 3423.
[38] A. Vallés, G. Jiménez, L. J. Salazar-Serrano, J. P. Torres, *Phys. Rev. A* **2018**, *97*, 023824.
[39] A. V. Paterova, H. Yang, C. An, D. A. Kalashnikov, L. A. Krivitsky, *Quantum Sci. Technol.* **2018**, *3*, 025008.
[40] A. Vanselow, P. Kaufmann, I. Zorin, B. Heise, H. M. Chrzanowski, S. Ramelow, *Optica* **2020**, *7*, 1729.